This document is confidential and is proprietary to the American Chemical Society and its authors. Do not copy or disclose without written permission. If you have received this item in error, notify the sender and delete all copies.

Deciphering melatonin-mediated micro and nanoscopic phase separation in phospholipid bilayers

Journal:	*Langmuir*
Manuscript ID	la-2019-01534q
Manuscript Type:	Article
Date Submitted by the Author:	22-May-2019
Complete List of Authors:	Bolmatov, Dima; Oak Ridge National Laboratory, Neutron Scattering Division McClintic, William; University of Tennessee Taylor, Graham; University of Tennessee Stanley, Christopher; Oak Ridge National Laboratory, Do, Changwoo; Oak Ridge National Laboratory, Biology and Soft Matter Division Collier, C.; Oak Ridge National Laboratory, Center for Nanophase Materials Sciences Leonenko, Zoya; University of Waterloo, Physics/Biology Lavrentovich, Maxim; University of Tennessee Katsaras, John; Oak Ridge National Laboratory, Neutron Sciences Directorate

SCHOLARONE™
Manuscripts

Deciphering melatonin-mediated micro and nanoscopic phase separation in phospholipid bilayers

Dima Bolmatov,[*,†,‡] William T. McClintic,[¶] Graham Taylor,[¶] Christopher B. Stanley,[§] Changwoo Do,[†] C. Patrick Collier,[∥] Zoya Leonenko,[⊥,#] Maxim O. Lavrentovich,[*,‡] and John Katsaras[†,‡]

† *Large Scale Structures Group, Neutron Scattering Division, Oak Ridge National Laboratory, Oak Ridge, TN 37831, United States*

‡ *Department of Physics and Astronomy, University of Tennessee, Knoxville, TN 37996, United States*

¶ *The Bredesen Center for Interdisciplinary Research, University of Tennessee, Knoxville, TN 37996, United States*

§ *Computational Sciences and Engineering Division, Oak Ridge National Laboratory, Oak Ridge, TN 37831, United States*

∥ *Center for Nanophase Materials Sciences, Oak Ridge National Laboratory, Oak Ridge, Tennessee 37831, United States*

⊥ *Department of Biology, University of Waterloo, 200 University Avenue West, N2L 3G1 Waterloo, ON, Canada*

\# *Department of Physics and Astronomy, University of Waterloo, 200 University Avenue West, N2L 3G1 Waterloo, ON, Canada*

E-mail: d.bolmatov@gmail.com; mlavrent@utk.edu

Abstract

Lipid bilayers are fundamental building blocks of cell membranes, which contain the necessary machinery to perform a range of biological functions, including cell-cell recognition, signal transduction, receptor trafficking, viral budding and cell fusion. Importantly, many of these functions are thought to take place in the phase separated regions of the membrane (i.e., lipid rafts). Here, we provide experimental evidence for the stabilizing effect of melatonin, a naturally occurring hormone produced by the brain's pineal gland, on phase separated phospholipid membranes composed of saturated 1,2-distearoyl-sn-glycero-3-phosphocholine (DSPC), unsaturated 1-palmitoyl-2-oleoyl-sn-glycero-3-phosphocholine (POPC) and 1,2-dioleoyl-sn-glycero-3-phosphocholine (DOPC), and cholesterol. Specifically, we show that melatonin stabilizes the liquid-ordered/liquid-disordered phase coexistence over an extended range of temperatures. Melatonin also causes the lipid bilayers to thin implying that this effect may play an important role in the membrane antioxidant abilities. The melatonin-mediated stabilization effect is observed in both nanometer and micrometer sized liposomes using small angle neutron scattering (SANS), confocal fluorescence microscopy, and differential scanning calorimetry. To experimentally detect nanoscopic domains in 50 nm diameter phospholipid vesicles, we develop a new model. Importantly, this model may serve as a platform in deciphering nanoscopic lateral heterogeneities in soft and biological materials with spherical and planar geometries in the presence of proteins, hormones, peptides, pathogens and other biomolecules.

Phase separation is an important physical feature for a range of processes,[1–9] including the compartmentalization of a biological solution into immiscible liquid components.[10–12] It can be induced through changes in pressure, temperature, concentration, and other thermodynamic and physicochemical parameters.

In biological systems, this liquid-liquid co-existence has been observed and is associated with a spectrum of biological processes.[13–15] For example, cells compartmentalize chemical reactions in order to facilitate the spatiotemporal regulation of cellular functions. Many of

the biological condensates in the cytoplasm and nucleoplasm resulting from phase separation are liquids[16] and are known to perform functions such as restructuring the genome[17] and repairing DNA.[18] Certain organelles and nuclear bodies also form through liquid-liquid phase separation during, for example, meiosis in developing embryos,[19] forming structures resembling oily microemulsions in water. Liquid-liquid phase separation may also describe the aggregation of intrinsically disordered proteins, which are relevant for the formation of structures like P granules[16,20] and are associated with diseases such as Alzheimer's. In the case of Alzheimer's, it is thought that Tau proteins undergo liquid-liquid phase separation, forming liquid protein droplets that trigger the disease.[21]

Biological membranes are underpinned by a lipid bilayer made up of lipids, amphipathic molecules, with different hydrophilic headgroups and hydrophobic fatty acid chains. To a great extent, the lipid bilayer is responsible for cell membrane structure and dynamics.[22–24] Importantly, lipid bilayers (i.e., cell membranes) are not laterally homogeneous, and their heterogeneity in model systems depends on pH, temperature, pressure, ionic strength, etc. Phase separation in biological membranes has been implicated in biological processes such as viral budding, cell fusion and cell-cell communication.[25–27] With regard to technological applications, targeted phase separated liposomes with a greater ability to fuse with other membranes have been used to deliver their payloads with greater efficacy.[28] As the direct observation of lipid rafts or domains in living cellular membranes is still a challenging and elusive task, model lipid membranes have been widely used as a good approach to study phase separation in membranes.

In the current work we looked into the effect that melatonin,[29] a hormone produced by the brain's pineal gland, affects phase separation in model membranes at length scales from the nanometer to the micrometer and at different temperatures. Melatonin is a biomolecule of great interest as it is believed to be an antioxidant, plays a role in regulating the sleep cycle,[29] and proposed to protect against different diseases,[30] including cardiovascular,[31] Alzheimer's[32] and certain types of cancers.[33] Moreover, clinical trials in humans have re-

ported mixed effects of melatonin on short-term cognitive functions[34] – as we age, our bodies make less melatonin, and its production is particularly impaired in those with Alzheimer's and other dementias.[35,36] Because of melatonin's physiological importance, and the fact that it is associated with membranes, it was obvious to undertake a study of how it affects biological membranes, in particular their lateral organization. Although there have been numerous membrane studies involving melatonin,[35] few have focused systematically on the effects of melatonin on phase separation within the membrane.

We used fluorescence microscopy, small angle neutron scattering (SANS), and differential scanning calorimetry to study the effect of melatonin on phase separation in nanoscopic unilamellar vesicles (ULVs) and macroscopic giant unilamellar vesicles (GUVs). We found that, irrespective of size, melatonin stabilizes lipid phase separation over a range of temperatures. We also developed a scattering model to identify lipid phase separation using the Landau-Brazovskii approach.[3]

Micrometer length scale lipid phase separation. A multi-component lipid mixture can exist in the plane of the membrane as an isotropically liquid disordered L_d phase (i.e., entropy exceeds the heat of mixing) or as a coexistence of liquid ordered L_o and liquid disordered L_d phases (i.e., heat overcomes entropy of mixing). We used GUVs, commonly used to study lipid phase separation on micrometer length scales[37] and confocal fluorescence microscopy to examine a well-known 4-component lipid mixture composed of 1,2-distearoyl-sn-glycero-3-phosphocholine (DSPC, 39 mol%), 1-palmitoyl-2-oleoyl-sn-glycero-3-phosphocholine (POPC, 33 mol%), 1,2-dioleoyl-sn-glycero-3-phosphocholine (DOPC, 6 mol%), and cholesterol (Chol, 22 mol%).[38,39] The L_o phase is characterized by a high degree of acyl-chain ordering (see Figure 1), while those of the coexisting disordered L_d phase are described by a higher degree of disorder. The L_o-L_d phase bilayers at 25°C have bilayer thicknesses that are mismatched,[38] including their bending moduli,[39] contributing to a reduced line tension. At 45°C, bilayers without melatonin undergo a phase transition from the L_o-L_d phase to the isotropically liquid disordered, L_d, phase. The lipid lateral diffusion,[24] which is

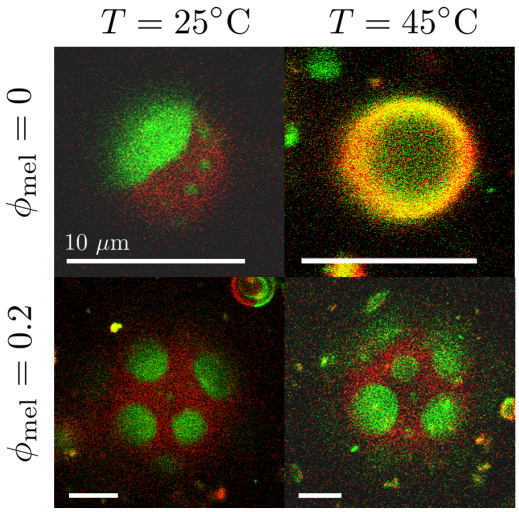

Figure 1: Confocal fluorescence microscopy of micrometer-sized GUVs. Macroscopic domain formation in a 4-component lipid mixture with (0.2 or 20 mol% melatonin) and without (0 mol%) melatonin at 25°C. At 45°C, domains coalesce forming a single liquid disordered phase. However, melatonin stabilizes the domains over a range of temperatures (up to 45°C), preventing the formation of the L_d phase.

moderately restricted at 25°C, increases at 45°C, and the bilayer's acyl chains become highly disordered, leading to the formation of the L_d phase. The addition of 20 mol% melatonin stabilizes the L_o-L_d phase, possibly through a reduced line tension, and domains are observed up to 45°C. This implies that the lipid headgroup-anchored melatonin molecules[40] may act as surfactants at L_o-L_d interfaces, a notion that we plan to explore in future studies. Our results (see Figure 1) are consistent with those from previous studies that have shown that surfactants in extracellular membranes lead to the formation of L_o-L_d phases at physiological temperatures.[41]

Zooming in on nanoscopic lipid phase separation. Vesicle finite size effects and their role in nanoscopic lipid phase separation have yet to be explored thoroughly.[42] This is because there are few techniques capable of studying nanoscopic materials under physiologically relevant conditions. SANS is inherently a nanoscopic technique and contrast matching approaches have been used to highlight different parts of lateral membrane structure.[38] Importantly, SANS is among the few techniques capable of providing nanoscale structural and dynamical[38,39] information without the need of extrinsic probes (e.g., fluorescent labels) that

are sometimes known to alter the interactions responsible for domain formation.

The coherent neutron scattering differential cross section for polydisperse ULVs with a uniform number density n is fully specified by the vesicle form factor, $F(\mathbf{q})$, and structure factor, $S(\mathbf{q})$. This is written as:[43]

$$\frac{d\Sigma}{d\Omega}(\mathbf{q}) = n\langle|F(\mathbf{q})|^2\rangle \left[1 + \frac{|\langle F(\mathbf{q})\rangle|^2}{\langle|F(\mathbf{q})|^2\rangle}\left(S(\mathbf{q}) - 1\right)\right], \tag{1}$$

where the averages $\langle\ldots\rangle$ are ensemble averages over many vesicles, which can vary in size (i.e., polydisperse). The form factor is given by:

$$F(\mathbf{q}) = -\int \mathrm{d}\mathbf{r}\,[\rho(\mathbf{r}) - \rho_s]\,e^{-i\mathbf{q}\cdot\mathbf{r}}, \tag{2}$$

where ρ_s is the scattering length density, SLD, of the solvent and $\rho(\mathbf{r})$ is the vesicle SLD.[44] For a dilute solution of vesicles, we can approximate $S(\mathbf{q}) \approx 1$, by ignoring the vesicle-vesicle interactions that contribute to the scattering. Our SANS experiments were performed using a dilute aqueous solution, thus we are only concerned with the spherically averaged intensity $I(q)$ that depends on the magnitude of the wave-vector $q = |\mathbf{q}|$, which is related to the neutron wavelength λ and the scattering angle θ according to: $q = (4\pi/\lambda)\sin(\theta/2)$. Therefore, the scattered intensity is an orientationally-averaged cross section. For a dilute solution of vesicles it can be written as:

$$I(q) = \frac{I_0}{4\pi}\int \langle|F(\mathbf{q})|^2\rangle\,\mathrm{d}\Omega_{\mathbf{q}} + I_{\text{inc.}}, \tag{3}$$

where $I_{\text{inc.}}$ is the q-independent incoherent scattering contribution and $I_0 \propto n$ is the overall vesicle density-dependent amplitude for the scattering intensity. The SANS experiment averages over all directions $\Omega_{\mathbf{q}}$ of the wave-vector $\mathbf{q}$.

The ensemble average in $\langle|F(\mathbf{q})|^2\rangle$ includes an average over some thermal distribution of ULVs – i.e., our scattering experiment is carried out at fixed temperature, T. Moreover,

the extrusion process used to generate ULVs results in vesicles with a narrow distribution of sizes or radii, R. Therefore, we average over the polydispersity and rewrite the averaged scattered intensity as:

$$\langle |F(\mathbf{q})|^2 \rangle = \int_0^\infty P(R) \, \langle |F_R(\mathbf{q})|^2 \rangle \, \mathrm{d}R, \tag{4}$$

where $P(R)$ is a probability distribution of ULVs with radius R, and $F_R(\mathbf{q})$ is the form factor. Experiments using extruded ULVs have shown[45] that the Shultz distribution is a physically reasonable descriptor of ULV polydispersity, i.e.:

$$P(R) = \left[\frac{z+1}{\bar{R}}\right]^{z+1} \frac{R^z}{\Gamma(z+1)} \exp\left[-\frac{R(z+1)}{\bar{R}}\right], \tag{5}$$

where $\bar{R}$ is the average ULV radius and z parameterizes the distribution variance: $\sigma_R^2 = \bar{R}^2/(z+1)$. This completes the description of the major points of the scattering theory. At this point, all that remains is to develop a physically justified scattering model for the form factor $F_R(\mathbf{q})$. Moreover, we distinguish between our high- and low-q SANS data.

Low-q scattering model vs SANS measurements. We studied $\bar{R} = 25$ nm ULVs with the same composition as was used for the GUVs in the optical measurements: i.e., DSPC (39 mol%), POPC (33 mol%), DOPC (6 mol%), and Chol (22 mol%). However, in order to make the ULVs "invisible" to neutrons at 45°C, a fraction of the DSPC lipids were deuterated (DSPC-protiated – 34.6%, DSPC-d_{70} – 65.4%) (see **Methods** for more details). In other words, at high T, when the lipid composition is spatially homogeneous (i.e., L_d phase) this composition leads to the absence of the scattering signal, implying that the lipids are well mixed[38] and $I(q) = I_{\text{inc.}}$. However, at low temperatures (i.e., 25°C), the membrane contains lateral inhomogeneities (i.e., domains) and $\rho(\mathbf{r}) - \rho_{\text{s}} \neq 0$ within the membrane. We can approximate these spatial variations as follows:

$$\rho(\mathbf{r}) \equiv \psi(\theta, \phi) \left[\Theta(r - R + t/2) - \Theta(r - R - t/2)\right], \tag{6}$$

where $\Theta(x) = 0$ for $x \leq 0$ and $\Theta(x) = 1$ for $x > 0$ is the Heaviside step function, and $\psi(\theta, \phi)$ is the lateral SLD variation. We use a "top-hat" function to represent the SLD contrast in the radial direction. This particular choice, however, does not alter the fits to the data in any remarkable way, as the low-q features are dominated by $\psi(\theta, q)$. Here, t represents the lipid bilayer thickness and it is convenient to expand $\psi(\theta, \phi)$ using spherical harmonics:

$$\psi(\theta, \phi) = \sum_{\ell,m} \psi_m^\ell Y_m^\ell(\Omega_{\mathbf{r}}), \tag{7}$$

where Y_m^ℓ is the spherical harmonic with angular momentum quantum number $\ell = 0, 1, 2, \ldots$ and azimuthal quantum number $m = -\ell, -\ell + 1, \ldots, \ell$. To calculate the form factor, we expand the Fourier component $e^{-i\mathbf{q}\cdot\mathbf{r}}$ as:

$$e^{-i\mathbf{q}\cdot\mathbf{r}} = 4\pi \sum_{\ell=0}^{\infty} \sum_{m=-\ell}^{\ell} (-i)^\ell j_\ell(qr) Y_\ell^m(\Omega_{\mathbf{q}}) [Y_\ell^m(\Omega_{\mathbf{r}})]^*, \tag{8}$$

where $j_\ell(x)$ is the spherical Bessel function.[46] The form factor now reads as:

$$F(\mathbf{q}) = 4\pi \sum_{\ell,m} \left[\int_{R-\frac{t}{2}}^{R+\frac{t}{2}} \mathrm{d}r\, r^2 j_\ell(qr) \right] \psi_m^\ell (-i)^\ell Y_m^\ell(\Omega_{\mathbf{q}}) \tag{9}$$

and the scattering intensity takes the form:

$$I = 4\pi I_0 \sum_{\ell,m} \left\{ \int_0^\infty P(R) \left[\Xi_\ell^{R,t}(q) \right]^2 \mathrm{d}R \right\} \langle |\psi_m^\ell|^2 \rangle + I_{\text{inc.}}, \tag{10}$$

where $I_0 \propto n$ is the overall vesicle concentration-dependent amplitude. We also obtain the

radial integration result in the closed form:

$$\begin{aligned}\Xi_\ell^{R,t}(q) &\equiv \int_{R-\frac{t}{2}}^{R+\frac{t}{2}} \mathrm{d}r\, r^2 j_\ell(qr) \\ &= \frac{\sqrt{\pi}\, q^\ell}{2^{\ell+1}\Gamma\left(\ell+\frac{3}{2}\right)(\ell+3)}\Bigg\{\left(R+\frac{t}{2}\right)^{\ell+3} {}_1F_2\left[\frac{\ell+3}{2};\ell+\frac{3}{2},\frac{\ell+5}{2};-\frac{q^2}{4}\left(R+\frac{t}{2}\right)^2\right] \\ &\quad -\left(R-\frac{t}{2}\right)^{\ell+3} {}_1F_2\left[\frac{\ell+3}{2};\ell+\frac{3}{2},\frac{\ell+5}{2};-\frac{q^2}{4}\left(R-\frac{t}{2}\right)^2\right]\Bigg\}, \qquad (11)\end{aligned}$$

where $\Gamma(x)$ is the gamma function and ${}_1F_2(a;b,c;z)$ is the generalized hypergeometric function. At this point, it is important to develop an appropriate model for $\langle|\psi_m^\ell|^2\rangle$. When the ULVs are at 45°C and all domains have melted, we have $\rho_{\mathrm{hc}} = \rho_{\mathrm{s}}$, where ρ_{hc} is the SLD of hydrocarbon acyl chains. As the temperature is lowered, the lipids will phase separate, but as no new material is added or removed from the lipid membrane, we expect SLD integrated over the entire ULV to remain the same. Therefore, for all temperatures we expect $\ell = 0$ mode to vanish, since we have:

$$\int \mathrm{d}\Omega_{\mathbf{r}}\left[\rho(\mathbf{r}) - \rho_{\mathrm{s}}\right] = \psi_0^0 = 0 \qquad (12)$$

Therefore, $\ell = 0$ is absent in our expansion and domains are expected to form when $\ell \neq 0$. Note, that domains have been observed for this particular lipid mixture in our optical microscopy data (see Figure 1) and in previous SANS experiments using similar size ULVs.[38] When domains form, there will be some SLD contrast variation at a length scale λ_0 on the surface of the spherical vesicle, which will correspond to an angular momentum mode: $\ell_0 \approx 2\pi R/\lambda_0$. We propose a model to describe lateral heterogeneities through $\psi(\theta,\phi)$, representing a phase-separating field with a Landau-Brazovskii type free energy.[47] This approach describes spatially modulated phases, which are ubiquitous in soft matter systems.[48] For instance, they are thought to arise when lipid membrane shape is coupled to a phase-separating lipid composition,[49] by varying the membrane thickness and bilayer

asymmetry. This mathematical formalism is general and has been successfully used to describe pollen grain pattern formation,[3,8] lipid domains on spherical vesicles,[50] viral capsid formation,[51] and block-copolymer assembly on a sphere.[52] Recent coarse-grained computer simulations of lipid bilayers have also suggested that domain formation can be thought of as a curvature-induced microemulsion.[53] Based on this prior evidence, we thought it appropriate to incorporate the Landau-Brazovskii approach into the framework of our scattering model. In our scattering model, the correlations of the spherical harmonic modes are given by:

$$\langle |\psi_m^\ell|^2 \rangle = \frac{\alpha}{(\ell^2 - \ell_0^2)^2 + R^2/\xi^2}, \tag{13}$$

where α is the overall amplitude and ξ is the temperature-dependent correlation length. This form is what one would expect in the disordered region of the modulated phase diagram, i.e., in a microemulsion phase. In an ordered modulated phase, there would be a large component of the scattering at a single $\ell = \ell_0$, representing a single domain size. However, as we shall see later, our results are more consistent with a range of domain sizes more consistent with a disordered phase. Also, when λ_0 becomes comparable to the vesicle radius, this model becomes essentially indistinguishable from an Ising-like model of phase separation, which may also be relevant for phase separated lipid systems.[54] In other words, the membrane could be phase-separated, but as the liquid ordered and liquid disordered phases coarsen, eventually they will merge and form a single domain on the ULV. As we will see, our SANS results are consistent with both scenarios, i.e., that of a microemulsion with a large λ_0 or a simple phase-separated vesicle – more detailed studies would be needed to differentiate between them experimentally. Substituting Eq. (13) into Eq. (10), we obtain a scattering model to describe the overall scattering density that reads:

$$I(q) = I_{\text{inc.}} + A \sum_{\ell=1}^{\infty} \int_0^\infty \frac{4\pi(2\ell+1)P(R)[\Xi_\ell^{R,t}(q)]^2}{(\ell^2 - 4\pi^2 R^2/\lambda_0^2)^2 + R^2/\xi^2}\, \mathrm{d}R, \tag{14}$$

where $A \propto n\alpha$ is the overall scattering amplitude that needs to be fitted. For this model of the scattered intensity there are seven parameters: A, λ_0, ξ, $I_{\text{inc.}}$, $\bar{R}$, z, and t. The integration over the radius distribution, $P(R)$, cannot be done analytically and needs to be approximated. This is done by approximating the integral using the trapezoidal rule, 10 segments, and an integration range from $\bar{R} - 2\sigma_R$ to $\bar{R} + 2\sigma_R$, where $\sigma_R = \bar{R}/\sqrt{z+1}$. That is, for any function $f(R)$, and in the current case, the function multiplying $P(R)$ in the integration, we obtain:

$$\int_0^\infty P(R) f(R)\,\mathrm{d}R \approx \sum_{R=\bar{R}-\frac{\sigma_R}{2}}^{\bar{R}+\frac{\sigma_R}{2}-\Delta R} \left[\frac{P(R+\Delta R)f(R+\Delta R) + P(R)f(R)}{2}\right]\Delta R, \tag{15}$$

with $\Delta R = 2\sigma_R/10$. We examined this solution using a finer partition or extending the integration interval, with similar results.[55]

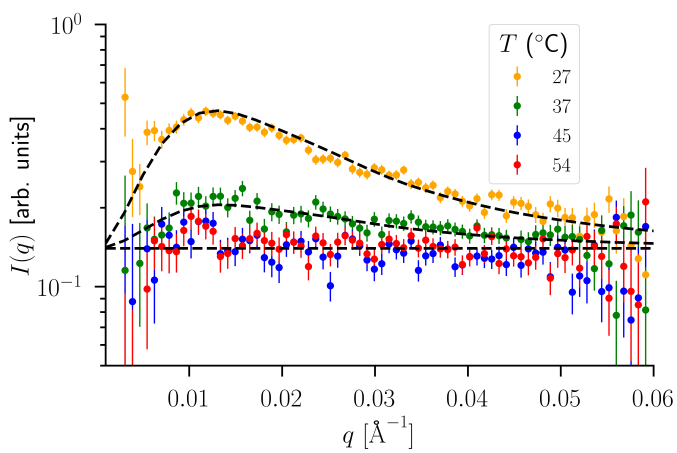

Figure 2: SANS intensities of 50 nm diameter ULVs for $\phi_{\text{mel.}} = 0$ mol%. $T = 45,\ 54$ °C scattering curves are basically featureless, consistent with pure incoherent scattering, $I_{\text{inc.}} = 0.14$ which we used to fit the two lower temperature data. For those data we estimated polydispersity parameters $z = 15$ and $\bar{R} = 250$ Å, which we estimated from the pore size of the filters used to extrude the ULVs and consistent with previously published data.[55] Finally, We performed a non-linear least-squares fit to the data by varying the parameters, A, ξ, and λ_0. The best fit values are given in Table 1.

Some of our fit parameters are known from independent experiments. Specifically, the diameter of ULVs is known by the pore size of the the polycarbonate filters used to extrude them ($\bar{R} = 25$ nm), and the lipid bilayer thickness, t, is known to be approximately 4 nm. We note that at low-q, ULV polydispersity can significantly modify the scattering curve, and a good estimate of $\bar{R}$ and z are important as the fitting procedure is particularly sensitive to the values of these parameters, unlike the case of the high-q data, where the scattering curve is much less affected by z and $\bar{R}$. So, we allowed z and $\bar{R}$ to vary in the fits, and then used the fixed estimates of $z = 15$ and $\bar{R} = 25$ nm for subsequent fits to all of our data, as the extrusion process was the same in all cases and we expected z and $\bar{R}$ to be the same for all the low-q samples. Finally, the $I_{\text{inc.}}$ can be estimated from the high temperature scattering data, where the SLDs of the solvent and ULVs are matched, resulting only in incoherent scattering. From the high temperature data, we estimate $I_{\text{inc.}} \approx 0.14$. The final fits presented in Fig. 2 for the low-q scattering data, then, had only three parameters: A, λ_0, and ξ. It should also be pointed out that it is not trivial to analytically sum over all $\ell = 1, \ldots, \infty$. We therefore defined a cutoff value as $\ell_{\text{max}} = 14$ and tested it with increasing cutoff values to see any appreciably changes to the results using different cutoffs. We did not. Below we tabulate the data as a result of our fits to the two lowest temperature scattering data with lipid domains: For the highest two temperature intensities we used: $I(q) \approx I_{\text{inc.}} \approx 0.14$.

Table 1: Fit parameters for low-q data without melatonin in Figure 2. Certain parameters were fixed (f.) based on independent measurements or additional physical considerations as discussed in the main text.

T (°C)	A (arb. units)	λ_0 (Å)	ξ (Å)	z (f.)	$\bar{R}$ (Å, f.)	t (Å, f.)	$I_{\text{inc.}}$ (f.)
27	2.65×10^{-11}	1.75×10^{4}	14.4	15	250	40	0.14
37	8.95×10^{-12}	1.55×10^{3}	10.8	15	250	40	0.14

Our results in Figure 2 indicate that the vesicles do indeed phase separate at low temperatures and that the domain sizes in such phase-separated vesicles are comparable to the vesicle radius, as the scattering spectrum $I(q)$ is peaked at values of q consistent with domain sizes on the order of 10 nanometers. In particular, the fitting procedure found that

$\lambda_0 \gg \xi, R_0$ (see Table 1). In this parameter regime, it is difficult to distinguish between bilayers forming a microemulsion phase, a modulated phase, or an ordered, phase-separated phase. It is possible that the ULVs are somewhere in the vicinity of the Lifshitz point, where these different phases can coexist.[53] However, the finite size of the ULVs vesicle may obscure our ability to detect, for example, a large characteristic domain size.

High-q scattering model vs SANS measurements. For high-q SANS experiments

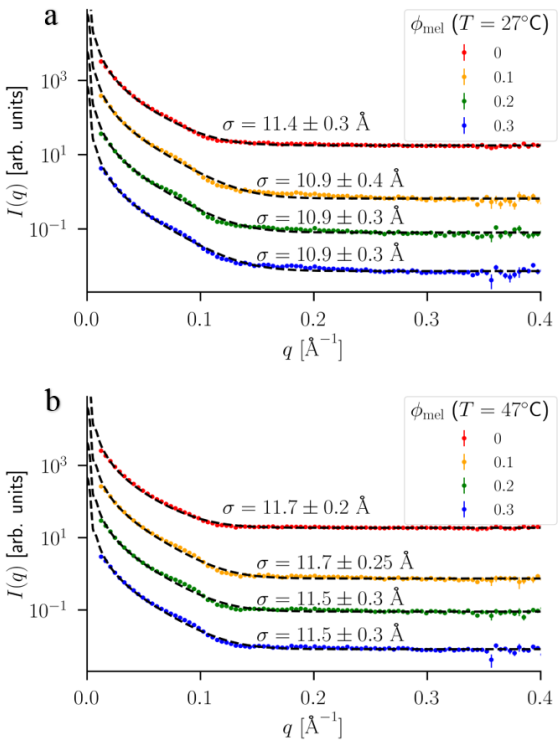

Figure 3: SANS high-q behavior of 100 nm diameter unilamellar vesicles. The effect of melatonin on membrane thickness, as denoted by σ at 27°C (a) and 47°C (b), respectively. Membrane thickness (i.e., σ) decreases with increasing amounts (0-30 mol%) of melatonin.

we extruded ULVs vesicles with $\bar{R} = 50$ nm and dispersed in a 100% D_2O solution, with an SLD of $\rho_s \approx 0.6$ fm/Å^3.[38] We assumed that the hydrocarbons of the lipid vesicle have an SLD of $\rho_{hc} \approx 0.2$ fm/Å^3 (see **Methods**). Therefore, the density contrast $|\rho(\mathbf{r}) - \rho_s|$ will vary from 0 (outside the membrane) to about 0.4 fm/Å^3 (near the center of the bilayer).[55] The value of z was fixed. Because of thermal fluctuations we model the lipid bilayer as a

Gaussian SLD contrast:

$$\rho(\mathbf{r}) - \rho_s = (\rho_{\mathrm{hc}} - \rho_{\mathrm{s}}) \exp\left[-\frac{(r-R)^2}{2\sigma^2}\right], \tag{16}$$

with $r \equiv |\mathbf{r}|$, R is the vesicle radius, and σ is a measure of bilayer thickness. The form factor can be evaluated exactly as follows:

$$\left\langle |F_R(q)|^2 \right\rangle = \frac{2\pi|\delta\rho|^2\sigma^2 e^{-q^2\sigma^2}}{q^2}\left[q\sigma^2\cos(qR) + R\sin(qR)\right]^2 \tag{17}$$

where $\delta\rho = \rho_{\mathrm{hc}} - \rho_{\mathrm{s}}$, and the scattered intensity can be represented as:

$$I(q) = A\int_0^\infty \left[\frac{\langle |F_R(q)|^2\rangle}{|\delta\rho|^2}\right] P(R)\,\mathrm{d}R + I_{\mathrm{inc.}}, \tag{18}$$

where $A \propto n|\rho_{\mathrm{hc}} - \rho_{\mathrm{s}}|^2$ is a parameter that incorporates the SLD contrast.[55] The value of z was fixed to the vesicle number density. Importantly, integrating over the Shultz distribution, $P(R)$, can be performed analytically, and $I(q)$ is fully specified and contains the following parameters: $\bar{R}$, σ, A, $I_{\mathrm{inc.}}$, and z. However, since $\bar{R}$ and z strongly depend on how the ULVs were prepared, these two parameters can be determined by other means. For the high-q measurements ULVs were fabricated using a polycarbonate filter with pores $\bar{R} = 50$ nm, and estimated $z = 15$ for the distribution, which gives a standard deviation of $\sigma_R = 12.5$ nm in ULV radius. This value for z is consistent with previous results.[55] z assumed a value of between 5 and 20, but was found to be rather insensitive to fitting the scattering data. Note that this same estimate of z was used in the low-q scattering fits.

We varied the melatonin concentration to see what effect it had on membrane thickness (see Figure 3), as measured via the parameter σ. We found that the best-fit-values of σ decrease with increasing levels of melatonin, i.e., the membranes got thinner. This result is in line with what has been published previously using homogeneous lipid mixtures,[56,57] which demonstrated decrease in membrane thickness. Importantly, melatonin-induced membrane

alteration is thought to protect against β-amyloid toxicity.[56] However, it would be interesting to understand how β-amyloid aggregation is influenced by the enhanced lipid phase separation in the presence of melatonin.

Low-q behavior in the presence of melatonin. In the presence of melatonin the lipid mixture SLD contrast was no longer matched as melatonin causes $\rho_{\text{hc}} \neq \rho_s$. Melatonin molecules are small, and localize below the lipid head group creating SLD contrast. To model this effect, we assumed that the melatonin localizes equally in both membrane leaflets, $R \pm \delta_{\text{mel.}}$, at the distance $\delta_{\text{mel.}}$ from the lipid bilayer center. Melatonin thus generates a Gaussian-shaped SLD contrast with a width $\sigma_{\text{mel.}}$. The scattering model then contains a homogeneous contribution from melatonin and an inhomogeneous contribution from the lipid domains and possibly of melatonin preferentially partitioning in the domains:

$$I = 4\pi A \int_0^\infty \left\{ \frac{2\rho_0^2 \sigma_{\text{mel.}}^2 e^{-q^2\sigma_{\text{mel.}}^2}}{q^2} \cos^2(q\delta_{\text{mel.}}) \left[(q\sigma_{\text{mel.}}^2 + \delta_{\text{mel.}} \tan(q\delta_{\text{mel.}})) \cos(qR) + R\sin(qR) \right]^2 \right.$$
$$\left. + \sum_{\ell=1}^{\ell_{\max}} \frac{(2\ell+1)[\Xi_\ell^{R,t}(q)]^2}{(\ell^2 - 4\pi^2 R^2/\lambda_0^2)^2 + R^2/\xi^2} \right\} P(R)\,\mathrm{d}R + I_{\text{inc,}} \tag{19}$$

where ρ_0 is the SLD contrast of melatonin and the solvent, which depends on melatonin concentration. Importantly, this scattering model introduces three additional melatonin-related parameters: ρ_0, $\delta_{\text{mel.}}$, $\sigma_{\text{mel.}}$. As in the low T results with no melatonin, we find that $\lambda_0 \gg \xi, \bar{R}$ for these scattering curves, implying that it is impossible to resolve a microemulsion phase from our data. Because the fitting procedure is not particularly sensitive to the choice of λ_0, as long as it is large compared to ξ and $\bar{R}$. So, we set $\lambda_0 = 10^4$ Å for fitting the data. $I_{\text{inc.}}$ was estimated independently by examining the large q scattering behavior, where the coherent scattering signal from the membrane is suppressed. Furthermore, we took into account that the melatonin resides somewhere below the head group in the lipid bilayer,[56,57] and set: $\delta_{\text{mel}} = 15$ Å. Moreover, as the melatonin molecules are small and would likely yield a localized SLD contrast just below the lipid headgroups, we set: $\sigma_{\text{mel.}} = 5$ Å.

As seen in Figure 4, our fitting results are consistent with lateral lipid phase separation

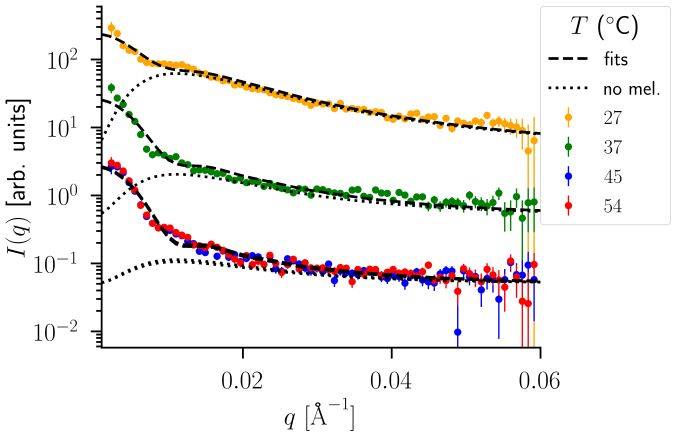

Figure 4: SANS intensities of 50 nm diameter unilamellar vesicles for $\phi_{\text{mel.}} = 10$ mol%. The curves are offset vertically for easier visualization. Importantly, the shoulder in the scattering data at around $q \approx 0.01$ Å^{-1} is consistent with lipid phase separation. However, this signal is overwhelmed at low-q due to increased scattering from melatonin. As in previous studies,[55] we estimated a polydispersity parameter $z = 15$ and $\bar{R} = 250$ Å . Additionally, due to the additional melatonin-related scattering parameters, we fixed $\lambda_0 = 10^4$ Å, as was determined in the experiments with no melatonin. Because of its magnitude, this parameter does not much influence the fitting results. We then performed a non-linear least-squares curve fitting by varying A, ξ, and ρ_0^2. The best-fit values of these parameters are listed in Table 2. Importantly, the dotted line, the result of lateral lipid phase separation, has a non-negligible contribution to all fits. Our results are therefore consistent with the presence of domains at given temperatures.

at low temperatures in the presence of melatonin. However, at high temperatures, although there is still some signal of phase separation, the scattering signal becomes overwhelmed by the presence of melatonin, which we expect to partially spoil our lipid contrast matching. This is evidenced by an excessive scattering signal at low-q, an effect previously observed in lipid phase-separated systems when $q \to 0$.[39] To determine if the scattering signal is still consistent with the presence of domains, we fixed $\xi = 16$ for the higher temperature data and let ρ_0^2 and $\sigma_{\text{mel.}}$ vary. In doing so, our fits to the data are consistent with the presence of lipid domains. However, a better contrast matching between melatonin and the lipids is needed in order to more definitively identify lateral phase separation.

Despite the issues with contrast matching due to melatonin "contamination" of the scattering signal, it seems that our data with melatonin is consistent with the presence of lipids

Table 2: Parameters used for fitting low-q neutron scattering data of lipid vesicles in the presence of melatonin (in Fig. 4). The "f." indicates that this parameter was fixed based on either independent measurements or additional considerations as discussed in the main text. In addition, we fixed the parameters $\lambda_0 = 10^4$ Å, $t = 40$ Å, $R = 250$ Å, and $z = 15$.

T (°C)	A (arb. units)	ξ (Å)	ρ_0^2	$\delta_{\text{mel.}}$ (Å, f.)	$\sigma_{\text{mel.}}$ (Å, f.)	$I_{\text{inc.}}$ (f.)
27	$(2.8 \pm 0.3) \times 10^{-11}$	16 ± 1	0.42 ± 0.06	5	15	0.05
37	$(7.6 \pm 0.6) \times 10^{-12}$	16 (f.)	3 ± 14	4 ± 8	15	0.05
45	$(2.7 \pm 0.7) \times 10^{-12}$	16 (f.)	1 ± 0.7	10	15	0.05
54	$(3.1 \pm 0.8) \times 10^{-12}$	16 (f.)	2 ± 12	7.2 ± 20	15	0.05

domains even at high T. To verify this statement we plotted the intensity curves with $\rho_0^2 = 0$ so that only the scattering signal originating from the lipids was detected (dotted lines in Figure 4). From this, it is clear that, for all temperatures, the scattered intensity curves are, at a minimum, consistent with a phase separated lipid bilayer. The various membrane parameters for the $\phi_{\text{mel}} = 10$ mol% case are presented in the Table 2.

In our future studies we will aim to better contrast melatonin in order to suppress its scattered signal that overwhelms the data at low-q. Ideally, contrast matching melatonin-containing bilayers can result in scattering curves not unlike those for the 0 mol% melatonin case at low temperatures (see Figure 2). Figure 5 shows the shape of the spherical harmonic mode distribution that is consistent with our SANS scattering data in which lipid domains were observed, i.e., low temperature ULVs without melatonin (see Figure 2) and ULVs with 10 mol% melatonin at low and high temperatures (see Figure 4). Note that this distribution is broad and has no particular characteristic mode. If the mode distribution was sharply peaked at a particular value of ℓ, we would expect to observe the type of modulated phases shown in the insets of Figure 5. Therefore, our scattering data is more consistent with a wide distribution of large lipid domain sizes (perhaps a microemulsion phase or almost fully phase-separated vesicles), rather than with an ordered modulated phase. Importantly, by studying this distribution for different lipid mixtures, it may become possible to search for modulated phases and the pattern formation at the nanoscale.

Finally, in Figure 6 we show differential scanning calorimetry (DSC) thermograms of

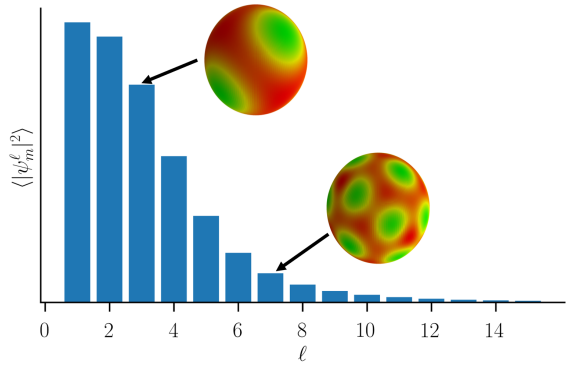

Figure 5: The spherical harmonic mode distribution. This distribution profile is consistent with SANS data from a phase separated membrane. Since we averaged over all ULV orientations, this profile is independent of m. In the insets to the figure we show how patterned states look like if the scattering distribution had a single peak at a value ℓ. Our result is consistent with a broad distribution of domain sizes with scattering contributions from many modes.

multilamellar vesicles (MLVs). DSC scans obtained in the case of 0 mol% melatonin are consistent with those from similar studies.[39] The thermotropic phase behavior of both hydrated MLV lipid dispersions (0 mol% and 20 mol%) exhibit slow kinetics towards their melting transition temperatures centred around $T_m \simeq 40°\mathrm{C}$, see Figure 6. Both thermograms are

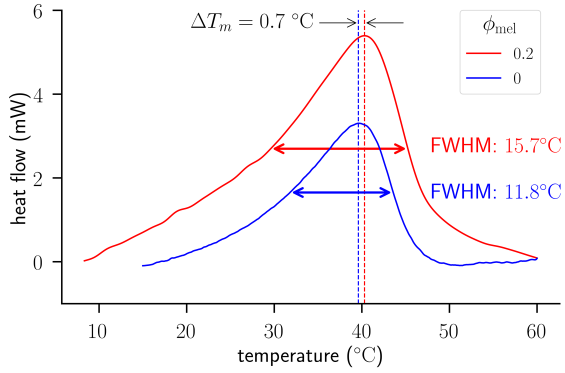

Figure 6: Differential scanning calorimetry thermograms of multilamellar vesicles. The presence of melatonin in lipid bilayers noticeably affects melting of lateral heterogeneities at intermediate and elevated temperatures.

noticeably broad, however, their effective melting ($T_{\mathrm{completion}} = T_m + \frac{T_{\mathrm{FWHM}}}{2}$, T_{FWHM} is the melting transition width, FWHM is the full width at half maximum[58]) completes at $\sim 45°\mathrm{C}$

(0 mol%) and $\sim 48°C$ (20 mol%), respectively. This implies that the 0 mol% melatonin-lipid mixture at 45°C is in the anharmonicity-facilitated isotropically liquid disordered state,[59] while the 20 mol% melatonin-lipid mixture is not completely melted (i.e. pre-melted) due to the presence of phase separated lateral heterogeneities, and, in fact, such structural heterogeneities may even persist in deep supercritical conditions.[60] In this regard, the DSC data is consistent with our fluorescence microscopy observations (see Figure 1). Importantly, the 0 mol% melatonin-lipid mixture undergoes very fast kinetics exhibiting a steep DSC slope beyond 45°C, see Figure 6, while DSC profile of the 20 mol% melatonin-lipid mixture undergoes a thermodynamic crossover at around 48°C followed by a "shoulder-like" slow kinetics towards $\sim 60°C$,[58] implying that this mixtures is still in the phase separated state at $T = 54°C$ (see Figure 6), and also consistent with our ULV SANS measurements (see Figures 2 and Figure 4).

In this study we presented experimental data revealing melatonin's ability to stabilize liquid-liquid phase separation in a biomimetic model system of lipid membranes composed of DSPC, POPC, DOPC and cholesterol. We used confocal fluorescence microscopy to image micrometer GUVs and SANS to explore nanometer ULVs with the same lipid composition as the GUVs. Importantly, we developed a scattering model to explain the lipid phase behavior, where lateral lipid heterogeneities were treated using the Landau-Brazovskii approach. The EQ-SANS instrument, see **Methods**, has the needed spatial resolution to detect nanoscopic domains in 50-100 nm diameter ULVs along with a direct measurement of membrane thickness. The microscopy and scattering data were further supported by DSC measurements.

The molecular basis of melatonin's domain stabilizing ability relies on the competitive forces between melatonin-lipid and lipid-lipid interactions. In phospholipids van der Waals forces are a substantial component of the intermolecular interactions,[40] and weaken near physiological temperatures.[22] As a result, the mobility of the lipids change and give rise to lipid behavior seen with increasing temperature.[22] However, melatonin-lipid interactions are noticeably stronger than the lipid-lipid interactions.[40] Specifically, melatonin strong inter-

actions with lipid headgroups are most likely responsible for melatonin's ability to stabilize lipid domains over a wide range of temperatures, as observed in this work using optical microscopy and SANS. In this regard, the thermodynamically stabilized lipid phase separation across different length scales is of particular interest, since phase separated lipid domains are implicated in myriad of physiological functions. Moreover, the observed membrane thinning effect may play an important role in their antioxidant abilities.[35]

Finally, our newly developed scattering model may serve as a platform in deciphering nanoscopic lateral heterogeneities in soft materials with spherical and planar geometries in the presence of proteins, hormones, peptides, pathogens and other biomolecules. Moreover, the use of the Landau-Brazovskii approach enables our scattering model to detect spatially modulated phases at the molecular level utilising x-ray or neutron scattering techniques.

Methods

Confocal Microscopy of GUVs. *Sample preparation.* GUVs were prepared by a modified electroformation procedure, as described in previous studies.[61] Lipid mixtures dissolved in chloroform and melatonin dissolved in 2,2,2-Trifluoroethanol (TFE, Sigma), at the appropriate mole fractions, were mixed and transferred to a conductive ITO slide (Delta-Technologies). Following transfer, the film-ITO slide was placed in vacuum for 1 hour to remove residual solvent. GUVs were swelled at 55°C in sucrose for 2 hours, and then cooled to room temperature. Electroformation parameters were set to 1V peak-to-peak at a frequency of 5 Hz. The GUV solution was then transferred to a PCR tube and GUVs were given 1 hour to settle prior to confocal microscopy imaging. Solutions were used within 24-48 hours of preparation.

Imaging. GUVs were imaged using a raster scanning, confocal microscope (Zeiss LSM T-PMT). A GUV solution was transferred to the center of a silicone gasket placed on a glass microscope slide. A glass cover slip was subsequently placed over the solution and the

silicone gasket. GUV images were collected using a 561 nm filter for exciting the DiI-C12 probe added to the film solution at a concentration of 0.05 mol%. A 405 nm filter was used to excite naphthopyrene that was added to the film solution at a concentration of 10 mol%. Importantly, the fluorescence spectrum of melatonin has maximum at ∼340 nm, significantly below the lower value cutoff filter.[62] DiI-C12 was chosen to selectively partition into the L_o phase of GUVs; naphthopryene was chosen to selectively partition into the L_d phase.[63] All GUVs were imaged using the red (DiI-C12) and blue (naphthopyrene) channels to check for partitioning of the corresponding dyes to the incorrect phase. For images viewed in the red channel, black regions of the membrane indicated a lack of illumination of the L_d phase-separated regions, and vice versa for the blue channel. This check, which indicates the integrity of the vesicles, was maintained under the light exposure.[64] GUV images were collected at 25°C and 45°C. The sample was given 15 minutes to equilibrate after a change in temperature.

SANS measurements of ULVs. *Sample preparation.* Unilamellar vesicles (ULVs) were prepared by extrusion, as previously described.[38,39] To study low-q behavior, we contrast matched the average SLD of the solvent, headgroup, and acyl chains using a 34.6% D_2O medium, and 65.4% of chain perdeuterated DSPC-d_{70},[38] as a percentage of total DSPC. Lipid mixtures were dissolved in chloroform and melatonin was dissolved in 2,2,2-Trifluoroethanol (TFE, Sigma). Samples were prepared by transferring desired volumes of solutions to a glass tube. Chloroform/Trifluoroethanol were removed with an N2 stream and moderate heating, and dried in vacuo for at least 12 hours. Dry lipid films were hydrated with an appropriate D2O/H2O mixture preheated to 50°C, followed by vortexing. The multilamellar vesicles (MLVs) were subsequently incubated at 50°C for 1 hour, followed by 5 freeze-thaw cycles between -80°C and 50°C.[38] ULVs were prepared with a miniextruder using polycarbonate filters with 50 or 100 nm pore-diameters heated to 50°C. The MLV solution was passed through the filter 31 times. The extruded samples were measured using SANS at 10-20 mg/mL concentrations within 24 hours of extrusion.

Measurements. SANS measurements were performed at the BL-6 Extended Q-range small angle neutron scattering (EQ-SANS) instrument of the Spallation Neutron Source (SNS), Oak Ridge National Laboratory (ORNL). ULVs were loaded into 1 mm path-length quartz banjo cells (Hellma USA, Plainview, NY) and mounted in a temperature-controlled cell holder with $\sim 1°$C accuracy. EQ-SANS data were collected at a 2.0 m SDD with a 2.5-5.5 Å wavelength band for a total scattering vector of $0.01 < q < 0.3$ Å^{-1}. The 2D SANS data were reduced using Mantid software.[65] During reduction, data were corrected for detector pixel sensitivity, dark current, sample transmission, and background scattering from water was subtracted.

Acknowledgements

We are indebted to Frederick A. Heberle, Milka Doktorova, Asja Radja, Haden Scott, Edward Lyman, and Philip Pincus for inspiring discussions. J. K. is supported through the Scientific User Facilities Division of the Department of Energy (DOE) Office of Science, sponsored by the Basic Energy Science (BES) Program, DOE Office of Science, under Contract No. DEAC05-00OR22725. M.O.L. gratefully acknowledges partial funding from the Neutron Sciences Directorate (Oak Ridge National Laboratory), sponsored by the US Department of Energy, Office of Basic Energy Sciences. A portion of this research at ORNL's Spallation Neutron Source was sponsored by the Scientific User Facilities Division, Office of Basic Energy Sciences, U.S. Department of Energy.

References

(1) Poole, P. H.; Sciortino, F.; Essmann, U.; Stanley, H. E. Phase behaviour of metastable water. *Nature* **1992**, *360*, 324.

(2) Bolmatov, D.; Brazhkin, V.; Trachenko, K. Thermodynamic behaviour of supercritical matter. *Nat. Commun.* **2013**, *4*, 2331.

(3) Lavrentovich, M. O.; Horsley, E. M.; Radja, A.; Sweeney, A. M.; Kamien, R. D. First-order patterning transitions on a sphere as a route to cell morphology. *Proc. Natl. Acad. Sci. U.S.A.* **2016**, *113*, 5189–5194.

(4) Bolmatov, D.; Zavyalov, D.; Zhernenkov, M.; Musaev, E. T.; Cai, Y. Q. Unified phonon-based approach to the thermodynamics of solid, liquid and gas states. *Ann. Phys.* **2015**, *363*, 221–242.

(5) Brangwynne, C. P.; Tompa, P.; Pappu, R. V. Polymer physics of intracellular phase transitions. *Nat. Phys.* **2015**, *11*, 899.

(6) Bolmatov, D.; Zhernenkov, M.; Zavyalov, D.; Tkachev, S. N.; Cunsolo, A.; Cai, Y. Q. The Frenkel Line: a direct experimental evidence for the new thermodynamic boundary. *Sci. Rep.* **2015**, *5*, 15850.

(7) Polymenidou, M. The RNA face of phase separation. *Science* **2018**, *360*, 859–860.

(8) Radja, A.; Horsley, E. M.; Lavrentovich, M. O.; Sweeney, A. M. Pollen Cell Wall Patterns Form from Modulated Phases. *Cell* **2019**, *176*, 856–868.

(9) Bolmatov, D.; Zhernenkov, M.; Zavyalov, D.; Stoupin, S.; Cai, Y. Q.; Cunsolo, A. Revealing the mechanism of the viscous-to-elastic crossover in liquids. *J. Phys. Chem. Lett.* **2015**, *6*, 3048–3053.

(10) Gerlich, D. W. Cell organization by liquid phase separation. *Nat. Rev. Mol. Cell Biol.* **2017**, *18*, 593.

(11) Strom, A. R.; Emelyanov, A. V.; Mir, M.; Fyodorov, D. V.; Darzacq, X.; Karpen, G. H. Phase separation drives heterochromatin domain formation. *Nature* **2017**, *547*, 241.

(12) Alberti, S.; Gladfelter, A.; Mittag, T. Considerations and challenges in studying liquid-liquid phase separation and biomolecular condensates. *Cell* **2019**, *176*, 419–434.

(13) Schwarz-Linek, J.; Valeriani, C.; Cacciuto, A.; Cates, M.; Marenduzzo, D.; Morozov, A.; Poon, W. Phase separation and rotor self-assembly in active particle suspensions. *Proc. Natl. Acad. Sci. U.S.A.* **2012**, *109*, 4052–4057.

(14) Nickels, J. D.; Chatterjee, S.; Stanley, C. B.; Qian, S.; Cheng, X.; Myles, D. A.; Standaert, R. F.; Elkins, J. G.; Katsaras, J. The in vivo structure of biological membranes and evidence for lipid domains. *PLOS Biol.* **2017**, *15*, e2002214.

(15) Bracha, D.; Walls, M. T.; Wei, M.-T.; Zhu, L.; Kurian, M.; Avalos, J. L.; Toettcher, J. E.; Brangwynne, C. P. Mapping local and global liquid phase behavior in living cells using photo-oligomerizable seeds. *Cell* **2018**, *175*, 1467–1480.

(16) Brangwynne, C. P.; Eckmann, C. R.; Courson, D. S.; Rybarska, A.; Hoege, C.; Gharakhani, J.; Jülicher, F.; Hyman, A. A. Germline P granules are liquid droplets that localize by controlled dissolution/condensation. *Science* **2009**, *324*, 1729–1732.

(17) Shin, Y.; Chang, Y.-C.; Lee, D. S.; Berry, J.; Sanders, D. W.; Ronceray, P.; Wingreen, N. S.; Haataja, M.; Brangwynne, C. P. Liquid nuclear condensates mechanically sense and restructure the genome. *Cell* **2018**, *175*, 1481–1491.

(18) Larson, A. G.; Elnatan, D.; Keenen, M. M.; Trnka, M. J.; Johnston, J. B.; Burlingame, A. L.; Agard, D. A.; Redding, S.; Narlikar, G. J. Liquid droplet formation by HP1α suggests a role for phase separation in heterochromatin. *Nature* **2017**, *547*, 236.

(19) Mitrea, D. M.; Kriwacki, R. W. Phase separation in biology; functional organization of a higher order. *Cell Commun. Signal.* **2016**, *14*, 1.

(20) Shin, Y.; Brangwynne, C. P. Liquid phase condensation in cell physiology and disease. *Science* **2017**, *357*, eaaf4382.

(21) Ambadipudi, S.; Biernat, J.; Riedel, D.; Mandelkow, E.; Zweckstetter, M. Liquid–liquid phase separation of the microtubule-binding repeats of the Alzheimer-related protein Tau. *Nat. Commun.* **2017**, *8*, 275.

(22) Kučerka, N.; Nieh, M.-P.; Katsaras, J. Fluid phase lipid areas and bilayer thicknesses of commonly used phosphatidylcholines as a function of temperature. *Biochim. Biophys. Acta Biomembr.* **2011**, *1808*, 2761–2771.

(23) Zhernenkov, M.; Bolmatov, D.; Soloviov, D.; Zhernenkov, K.; Toperverg, B. P.; Cunsolo, A.; Bosak, A.; Cai, Y. Q. Revealing the mechanism of passive transport in lipid bilayers via phonon-mediated nanometre-scale density fluctuations. *Nat. Commun.* **2016**, *7*, 11575.

(24) Bolmatov, D.; Cai, Y. Q.; Zavyalov, D.; Zhernenkov, M. Crossover from picosecond collective to single particle dynamics defines the mechanism of lateral lipid diffusion. *Biochim. Biophys. Acta Biomembr.* **2018**, *1860*, 2446–2455.

(25) Grakoui, A.; Bromley, S. K.; Sumen, C.; Davis, M. M.; Shaw, A. S.; Allen, P. M.; Dustin, M. L. The immunological synapse: a molecular machine controlling T cell activation. *Science* **1999**, *285*, 221–227.

(26) Chazal, N.; Gerlier, D. Virus entry, assembly, budding, and membrane rafts. *Microbiol. Mol. Biol. Rev.* **2003**, *67*, 226–237.

(27) Choi, K. S.; Aizaki, H.; Lai, M. M. Murine coronavirus requires lipid rafts for virus entry and cell-cell fusion but not for virus release. *J. Virol.* **2005**, *79*, 9862–9871.

(28) Imam, Z. I.; Kenyon, L. E.; Ashby, G.; Nagib, F.; Mendicino, M.; Zhao, C.; Gadok, A. K.; Stachowiak, J. C. Phase-Separated Liposomes Enhance the Efficiency

of Macromolecular Delivery to the Cellular Cytoplasm. *Cell. Mol. Bioeng.* **2017**, *10*, 387–403.

(29) Pandi-Perumal, S. R.; Trakht, I.; Spence, D. W.; Srinivasan, V.; Dagan, Y.; Cardinali, D. P. The roles of melatonin and light in the pathophysiology and treatment of circadian rhythm sleep disorders. *Nat. Rev. Neurol.* **2008**, *4*, 436.

(30) Ortiz, G. G.; Benítez-King, G. A.; Rosales-Corral, S. A.; Pacheco-Moisés, F. P.; Velázquez-Brizuela, I. E. Cellular and biochemical actions of melatonin which protect against free radicals: role in neurodegenerative disorders. *Curr. Neuropharmacol.* **2008**, *6*, 203–214.

(31) Sun, H.; Gusdon, A. M.; Qu, S. Effects of melatonin on cardiovascular diseases: progress in the past year. *Curr. Opin. Lipidol.* **2016**, *27*, 408.

(32) P Cardinali, D.; M Furio, A.; I Brusco, L. Clinical aspects of melatonin intervention in Alzheimer's disease progression. *Curr. Neuropharmacol.* **2010**, *8*, 218–227.

(33) Carbajo-Pescador, S.; Steinmetz, C.; Kashyap, A.; Lorenz, S.; Mauriz, J.; Heise, M.; Galle, P.; Gonzalez-Gallego, J.; Strand, S. Melatonin induces transcriptional regulation of Bim by FoxO3a in HepG2 cells. *Br. J. Cancer* **2013**, *108*, 442.

(34) Peck, J. S.; LeGoff, D. B.; Ahmed, I.; Goebert, D. Cognitive effects of exogenous melatonin administration in elderly persons: a pilot study. *Am. J. Geriatr. Psychiatry* **2004**, *12*, 432–436.

(35) García, J. J.; López-Pingarrón, L.; Almeida-Souza, P.; Tres, A.; Escudero, P.; García-Gil, F. A.; Tan, D.-X.; Reiter, R. J.; Ramírez, J. M.; Bernal-Pérez, M. Protective effects of melatonin in reducing oxidative stress and in preserving the fluidity of biological membranes: a review. *J. Pineal Res.* **2014**, *56*, 225–237.

(36) Vander Zanden, C. M.; Majewski, J. P.; Watkins, E. B.; Chi, E. Y. Synchrotron X-Ray Scattering Studies to Determine Structure of Amyloid Beta Interactions with Lipid Membranes. *Biophys. J.* **2019**, *116*, 45a.

(37) Veatch, S. L.; Keller, S. L. Miscibility phase diagrams of giant vesicles containing sphingomyelin. *Phys. Rev. Lett.* **2005**, *94*, 148101.

(38) Heberle, F. A.; Petruzielo, R. S.; Pan, J.; Drazba, P.; Kucerka, N.; Standaert, R. F.; Feigenson, G. W.; Katsaras, J. Bilayer thickness mismatch controls domain size in model membranes. *J. Am. Chem. Soc.* **2013**, *135*, 6853–6859.

(39) others,, et al. Mechanical properties of nanoscopic lipid domains. *J. Am. Chem. Soc.* **2015**, *137*, 15772–15780.

(40) Severcan, F.; Sahin, I.; Kazancı, N. Melatonin strongly interacts with zwitterionic model membranesevidence from Fourier transform infrared spectroscopy and differential scanning calorimetry. *Biochim. Biophys. Acta Biomembr.* **2005**, *1668*, 215–222.

(41) Casals, C.; Cañadas, O. Role of lipid ordered/disordered phase coexistence in pulmonary surfactant function. *Biochim. Biophys. Acta Biomembr.* **2012**, *1818*, 2550–2562.

(42) He, S.; Maibaum, L. Identifying the onset of phase separation in quaternary lipid bilayer systems from coarse-grained simulations. *J. Phys. Chem. B* **2018**, *122*, 3961–3973.

(43) Kotlarchyk, M.; Chen, S.-H. Analysis of small angle neutron scattering spectra from polydisperse interacting colloids. *J. Chem. Phys.* **1983**, *79*, 2461–2469.

(44) Anghel, V. N.; Bolmatov, D.; Katsaras, J. Models for randomly distributed nanoscopic domains on spherical vesicles. *Phys. Rev. E* **2018**, *97*, 062405.

(45) Pencer, J.; Krueger, S.; Adams, C. P.; Katsaras, J. Method of separated form factors for polydisperse vesicles. *J. Appl. Cryst.* **2006**, *39*, 293–303.

(46) Edmonds, A. R. *Angular momentum in quantum mechanics*; Princeton university press, 1996; Vol. 4.

(47) Brazovskiĭ, *Phase transition of an isotropic system to a nonuniform state*.

(48) Seul, M.; Andelman, D. Domain shapes and patterns: the phenomenology of modulated phases. *Science* **1995**, *267*, 476–483.

(49) Leibler, S.; Andelman, D. Ordered and curved meso-structures in membranes and amphiphilic films. *J. Physique* **1987**, *48*, 2013–2018.

(50) Luo, Y.; Maibaum, L. Phase diagrams of multicomponent lipid vesicles: Effects of finite size and spherical geometry. *J. Chem. Phys.* **2018**, *149*, 174901.

(51) Dharmavaram, S.; Xie, F.; Klug, W.; Rudnick, J.; Bruinsma, R. Orientational phase transitions and the assembly of viral capsids. *Phys. Rev. E* **2017**, *95*, 062402.

(52) Chantawansri, T. L.; Bosse, A. W.; Hexemer, A.; Ceniceros, H. D.; García-Cervera, C. J.; Kramer, E. J.; Fredrickson, G. H. Self-consistent field theory simulations of block copolymer assembly on a sphere. *Phys. Rev. E* **2007**, *75*, 031802.

(53) Sadeghi, S.; Müller, M.; Vink, R. L. Raft formation in lipid bilayers coupled to curvature. *Biophys. J.* **2014**, *107*, 1591–1600.

(54) Veatch, S. L.; Soubias, O.; Keller, S. L.; Gawrisch, K. Critical fluctuations in domain-forming lipid mixtures. *Proc. Natl. Acad. Sci. U.S.A.* **2007**, *104*, 17650–17655.

(55) Frisken, B.; Asman, C.; Patty, P. Studies of vesicle extrusion. *Langmuir* **2000**, *16*, 928–933.

(56) Drolle, E.; Kučerka, N.; Hoopes, M.; Choi, Y.; Katsaras, J.; Karttunen, M.; Leonenko, Z. Effect of melatonin and cholesterol on the structure of DOPC and DPPC membranes. *Biochim. Biophys. Acta Biomembr.* **2013**, *1828*, 2247–2254.

(57) Dies, H.; Cheung, B.; Tang, J.; Rheinstädter, M. C. The organization of melatonin in lipid membranes. *Biochim. Biophys. Acta Biomembr.* **2015**, *1848*, 1032–1040.

(58) Lewis, R. N.; Mannock, D. A.; McElhaney, R. N. *Methods in Membrane Lipids*; Springer, 2007; pp 171–195.

(59) Bolmatov, D.; Brazhkin, V.; Trachenko, K. The phonon theory of liquid thermodynamics. *Sci. Rep.* **2012**, *2*, 421.

(60) Bolmatov, D.; Zavyalov, D.; Gao, M.; Zhernenkov, M. Structural evolution of supercritical CO2 across the Frenkel line. *J. Phys. Chem. Lett.* **2014**, *5*, 2785–2790.

(61) Angelova, M.; Soléau, S.; Méléard, P.; Faucon, F.; Bothorel, P. *Trends in colloid and interface science VI*; Springer, 1992; pp 127–131.

(62) King, M.; Scaiano, J. The excited states of melatonin. *Photochem. Photobiol.* **1997**, *65*, 538–542.

(63) Baumgart, T.; Hunt, G.; Farkas, E. R.; Webb, W. W.; Feigenson, G. W. Fluorescence probe partitioning between Lo/Ld phases in lipid membranes. *Biochim. Biophys. Acta Biomembr.* **2007**, *1768*, 2182–2194.

(64) Morales-Penningston, N. F.; Wu, J.; Farkas, E. R.; Goh, S. L.; Konyakhina, T. M.; Zheng, J. Y.; Webb, W. W.; Feigenson, G. W. GUV preparation and imaging: minimizing artifacts. *Biochim. Biophys. Acta Biomembr.* **2010**, *1798*, 1324–1332.

(65) Arnold, O.; Bilheux, J.-C.; Borreguero, J.; Buts, A.; Campbell, S. I.; Chapon, L.; Doucet, M.; Draper, N.; Leal, R. F.; Gigg, M. MantidData analysis and visualization package for neutron scattering and μ SR experiments. *Nucl. Instrum. Methods Phys. Res.* **2014**, *764*, 156–166.
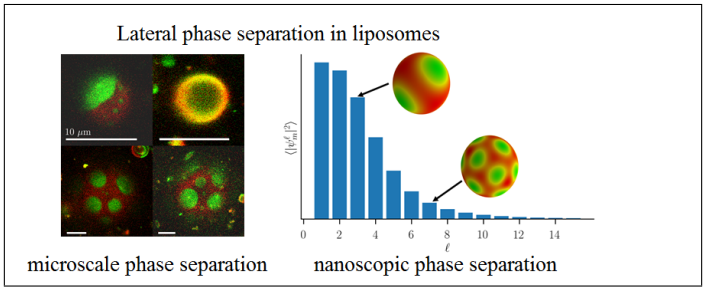
Graphical TOC Entry